Advanced Composites and Hybrid Materials (2022) 5:1841–1851
https://doi.org/10.1007/s42114-022-00460-z

ORIGINAL RESEARCH

Combined bactericidal process of lignin and silver in a hybrid nanoparticle on *E. coli*

Fangli Ran[1,2] · Chenyu Li[1] · Zhenxin Hao[1,2] · Xinyuan Zhang[1,2] · Lin Dai[2] · Chuanling Si[2] · Zhiqiang Shen[1] · Zhigang Qiu[1] · Jingfeng Wang[1,2]

Received: 25 January 2022 / Revised: 25 February 2022 / Accepted: 21 March 2022 / Published online: 12 April 2022

Abstract

Among multiple engineered nanoparticles that have been used in the bactericidal application, silver nanoparticles (Ag NPs) are the most explored bactericidal functional materials with their high efficiency and broad-spectrum bactericidal properties. However, environmental toxicology and lack of modifiability restrict their further development. In this study, a simple and economic method was established to fabricate lignin and silver hybrid nanoparticles (Lig-Ag NPs) with bactericidal ability. Afterwards, material characterization, bactericidal evaluation, and mechanism exploration were implemented to explore the properties of Lig-Ag NPs. The results indicated that Lig-Ag NPs not only demonstrated remarkable dispersity, uniformity, and encapsulation efficiency but also possessed approximated bactericidal ability on *Escherichia coli* and better durability compared with the same concentration of Ag NPs on *E. coli*. On the other hand, flow cytometry and transcriptomic analysis were used to further explore the bactericidal mechanism of Lig-Ag NPs. The results showed that oxidative stress was the possible leading bactericidal mechanism of Lig-Ag NPs. The formation approaches of reactive oxygen species production were various including the slow release of silver ion and generation of quinone/semi-quinone radicals on account of the combined effect of lignin and silver.

Keywords Lignin · Silver · Nanoparticles · *E. coli* · Oxidative stress

1 Introduction

The public panic about the widespread of COVID-19 has triggered recently a proliferated use of bactericidal products [1, 2]. In recent years, nanoparticles are heavily used to disinfect microorganisms due to their toxicological effect and small size effect [3–9]. Among multiple engineered nanoparticles that have been used in bactericidal application, silver nanoparticles (Ag NPs) are the most explored bactericidal functional materials with their high efficiency and broad-spectrum bactericidal properties [10–14]. However, the waste Ag NPs cannot recover or deactivate in refuse processing plants or sewage treatment plant [11]. As time goes on, the continuous exposure of Ag nanocore may lead to several ecological problems, such as the change of microbial community composition [15] and horizontal transfer of antibiotic resistance genes [16–18]. On the other hand, unmodified Ag NPs are hard to directly form applicable bactericidal products blaming on lack of an active group to chemical graft [19, 20]. Core–shell structure is an ideal solution to construct a more stable composition of Ag NPs materials. Khan et al. [21] established a novel bactericidal composite that was synthesized by coating ZnO on the surface of biogenic Ag nanoparticles which had been formed using the leaf extracts of *Hibiscus sabdariffa*. Guo et al. [22] synthesized core–shell Ag@ZIF-8 nanowires with bactericidal activity tested against *Bacillus subtilis* and *Escherichia coli BL21*, while these reported [23, 24] shell structures mostly acted as a protective layer of Ag NPs with mass transfer

✉ Chenyu Li
nk_lcy710430@hotmail.com

✉ Lin Dai
dailin@tust.edu.cn

✉ Jingfeng Wang
wangjingfeng0116@163.com

[1] Department of Environment and Health, Tianjin Institute of Environmental and Operational Medicine, Tianjin 300050, People's Republic of China

[2] Tianjin Key Laboratory of Pulp and Paper, College of Light Industry and Engineering, Tianjin University of Science and Technology, Tianjin 300457, People's Republic of China

resistance and theoretically had an obviously negative influence on bactericidal efficiency.

Lignin, a cheap, abundant, and green material, is the second-largest natural biopolymers on the earth and the main waste product from agro-waste and papermaking industries [25–31]. Nature lignin is known to possess many advanced properties, such as good bactericidal activity and antioxidant properties [32–35]. Therefore, in the area of antibacteria, lignin has been widely used as a potential matrix material. Chen et al. [36] used kraft lignin to prepare an aminated lignin-silver complex, which was proved as an ideal alternative bactericidal agent against gram-positive (*Bacillus cereus*, *Staphylococcus aureus*) and gram-negative (*Salmonella enterica*) bacteria. Li et al. [37] designed a lignin-based bactericidal hydrogel for antimicrobial application. The biocompatible hydrogel has good broad-spectrum bactericidal properties due to the enhanced bactericidal effect of both the hydrogel and silver nanoparticles. Wang et al. synthesized silver nanoparticles incorporated quaternized lignin (QAL) composites with the assistance of microwave radiation. Owing to the electrostatic effect of QAL on bacteria, Ag@QAL exhibits the highest antibacterial activity with 3.72 log10(> 99.9%) and 5.29 log10(> 99.999%) CFU/mL reduction against *E. coli* and *S. aureus*, respectively. But for all this, above synthesized composites had yet to verify those antibacterial abilities versus equivalent Ag NPs simple substance. On the other hand, the bactericidal mechanism needed to be further explored at a molecular level.

In this study, complex lignin-silver nanoparticles (Lig-Ag NPs) were synthesized with a core–shell structure. Industrial alkaline lignin was used to reduce silver ions (Ag^+) to Ag NPs in situ. The phenolic hydroxyls or methoxy groups on the lignin can reduce Ag^+ to metallic Ag NPs and then convert them to dynamically stable semi-quinone radicals. Lignin produced free radicals through REDOX, and silver ions released from Lig-Ag NPs played a positive role in the killing of *Escherichia coli* (*E. coli*), which achieved the bactericidal effect by inducing oxidative stress reaction and damage to the bacterial cell membrane. The shell structure helped to reduce the toxic effect of silver nanoparticles, and the bactericidal effect on *E. coli* was more durable than Ag NPs. Our results demonstrated that the application of green and facile design strategy may allow the synthesis of bactericidal agents with higher bactericidal activity and less environmental impact.

2 Experimental section

2.1 Chemicals and reagents

Alkaline lignin was kindly supplied by Shan Dong Sun Paper Industry Joint Stock Co., Ltd. Silver nitrate ($AgNO_3$) was obtained from Sinopharm Chemical Reagent CO., Ltd. (Shanghai, China). Ag NPs were purchased from Sigma-Aldrich, Co., Ltd. (< 100 nm particle size, 99.5% trace metals basis). Ammonium hydroxide ($NH_3{\cdot}H_2O$, AR) and sodium hydroxide (NaOH, AR) were purchased from the Damao Chemical Reagent Factory (Tianjin, China).

2.2 Preparation of bacteria

Escherichia coli K12-MG1655 (*ATCC 700,926*) were inoculated in Luria–Bertani broth (LB, Sangon Biotech, China) and cultured at 37 ℃ constant temperature shaker (THZ-82A, Tianjin Sateris Experimental Analysis Instrument Company, China), at 150 rpm for 12 h. The bacterial suspensions were centrifuged at 4629 *g* for 5 min (5804R, Eppendorf, Germany) and washed with phosphate-buffered saline (PBS, pH 7.2 ~ 7.4) 3 times to remove any broth medium residuals. In the end, bacterial cells were resuspended in PBS and stored at 4 ℃ for reserve.

2.3 Synthesis of Lig-Ag NPs

Lig-Ag NPs were fabricated by the nanoprecipitation method in an alkaline system with a reduction process. 0.2 g of alkaline lignin was fully dissolved in 4 mL of NaOH solution (5% w/v) by ultrasonic treatment for getting solution A. Subsequently, 5 mL of $AgNO_3$ solution (10 g/L Ag^+) was slowly added into 2.5 mL $NH_3{\cdot}H_2O$ (7.6% w/v) under magnetic stirring for getting solution B. Finally, solution A was dropwise added to solution B under magnetic stirring. The product was dialyzed in freshly deionized water for 3 days and made up to 100 mL with deionized water for getting Lig-Ag NPs stock solution.

2.4 Characterization

The microstructures of the samples were observed by field-emission scanning electron microscope (FE-SEM). The diluted and dispersed Lig-Ag NPs solution was dropped onto a silicon slice to prepare samples. After air-drying, in order to avoid charging effects, the samples were coated with platinum prior to FE-SEM analysis (Sigma 300, Zeiss, Germany) at an accelerating voltage of 5.00 kV. Element mapping analysis was carried out by an energy disperse spectroscopy [38] (EDS, Ultim Extreme, Oxford Instrument, UK).

For the bacterial suspension, the samples were dehydrated using graded ethanol and freeze-dried (FDU-1200, EYELA, Japan). Subsequently, platinum was used to coat samples for FE-SEM analysis. The particle size was analyzed by DLS (Malvern Nano-ZS Zeta Sizer, Malvern Instruments, UK). Lig-AP NPs were diluted with deionized water and ultrasonically dispersed for 3 min before analysis.

The wettability of Lig-Ag NPs and Ag NPs was investigated by determining the static water contact angel (WCA)

by a sessile drop method [39], employing an automated WCA apparatus (ZR-SDJ-B3, defnuo, China). For each measurement, 10 mL specific concentration Lig-Ag NPs or Ag NPs was dispersed over a piece of polyamide membrane. After airing, a deionized water droplet (~6.5 μL) was deposited onto the surface, and images were recorded to analyze WCA.

The chemical structures were confirmed by Fourier transform infrared (FT-IR), ultraviolet–visible (UV–vis), and X-ray photoelectron spectroscopy (XPS). Samples (Lig-Ag NPs and Lignin) were incorporated into KBr and pressed to formulate a 3-mm tablet by a table press (HY-12, Tianjin optical instrument factory, China). The infrared spectrum from 2000 to 400 cm was acquired from an FT-IR spectroscopy (Nicolet iS5, Thermo Scientific Co. Ltd., USA) operating at a resolution ratio of 2 cm^{-1}. Second-derivative spectra were obtained with the use of the Nicolet software (DR2, Thermo Scientific Co. Ltd., USA). For the UV–vis spectroscopy, lignin and Lig-Ag NPs suspension were diluted over the wavelength range from 200 to 800 nm using a UV–vis spectrometer (UV-2600, SHIMADZU, Japan). NaOH solution was used as a blank control group. XPS of samples (Lignin, Lig-Ag NPs, and Ag NPs) was detected by a photoelectron spectrometer (EscaLab Xi+, Thermo Scientific Co. Ltd., USA) with Al Kα radiation (1486.6 eV) and hemispherical electron energy analyzer. The radiation source operated at 14.4 kV and 13.6 mA. The vacuum pressure was kept around 8×10^{-10} pa all along. The binding energy scale was corrected by referring to the C1s spectrum as being 284.80 eV.

2.5 Evaluation the bactericidal ability of Lig-Ag NPs

0.2 ml of Lig-Ag NPs stock solution was added to 9.8 mL of bacterial suspension (about 1×10^7 CFU/mL), diluted from the bacterial stock solution with PBS to derive a final sliver concentration of 0, 0.5, 1, 5, and 10 mg/L. Meanwhile, Ag NPs and lignin experimental groups were prepared similarly, but with equal concentration Ag NPs or lignin instead of Lig-Ag NPs. All the bacterial suspensions were exposed to experimental materials on a constant temperature shaking table (HNYC-203 T, Honour Co. Ltd., China). After the designed exposure time, the live bacteria numbers were determined by counting the numbers of CFUs on solid LB agar plates, which were incubated at 37 ℃ for 16–18 h. The bacterial survival rate was expressed as N/N_0 (×100%), in which N and N_0 represent the remaining and initial numbers of live bacteria, respectively. In the performance attenuation experiments, the Lig-Ag NPs and Ag NPs were respectively placed in freshly deionized water for 3 months. Afterwards, the bactericidal materials were dialyzed for 3 days and ultrasonically dispersed for 3 min as well to test the bactericidal ability. In addition, ROS scavenger (*N*-acetyl-*L*-cysteine, 100 μM) to quantitatively analyze whether Lig-Ag NPs could inhibit *E.coli* growth or not via ROS generation.

2.6 Measurement of cell membrane permeability

Cell membrane permeability of *E. coli* was determined by using Syto-9 and propidium iodide (PI) dyes [40] (live/dead biofilm viability kit, Thermo Scientific Co. Ltd., USA). Briefly, *E. coli* suspensions were exposed to designed concentrations of bactericidal materials (Lig-Ag NPs and Ag NPs) for 2 h. Two milliliter of bacterial cells was stained with Syto-9/PI (100 μM) combination of dyes. Samples were kept at room temperature in the dark and incubated for 10 min and then immediately analyzed by flow cytometry. One hundred thousand events were analyzed. Forward scatter (FSC), green fluorescence (FL1 515–565 nm), and red fluorescence (FL3 > 605 nm) were measured using a flow cytometer (FCM, S3 cell sorter, Bio-rad Inc., USA). The FCM was equipped with 100 mW, 488 nm, solid laser. FSC characteristics were used as a trigger signal. Finally, data analysis was accomplished with FlowJo 10 (FLOWJO, LLC and BD Biosciences, USA). All samples were sorted by the same oval gate in scatter plots with FL1 *X*-coordinate and FL3 *Y*-coordinate.

2.7 RNA extraction, genome-wide sequencing, and transcriptomic analysis

The bactericidal systems were established as described above, with dosages of 5 mg/L Ag element within Lig-Ag NPs and Ag NPs. After 2 h of exposure, the samples were submitted to omics laboratory (Novogene Co., Ltd., China) for genome-wide RNA sequencing. The RNA samples were analyzed and subjected to quality control. After this, the cDNA libraries were constructed and sequenced on the Illumina NovaSeq6000 Platform (Illumina Inc., San Diego, CA). The fragments per kilobase of a gene per million mapped reads (FPKM) were measured to quantify the gene expression. Differences in the gene expression between the control and the Lig-Ag NPs and Ag NPs were presented as $\log_2$ fold changes of the averaged FPKM values.

2.8 Statistical analysis

All experiments were conducted independently at least in biological triplicate. Phenotypic data statistical analysis was performed using SPSS 25.0 (Chicago, USA) with analysis of variance (ANOVA) and independent-sample *t*-test methods and expressed as mean ± standard deviation (SD). The corrected p values of < 0.05 were considered to indicate statistical significance.

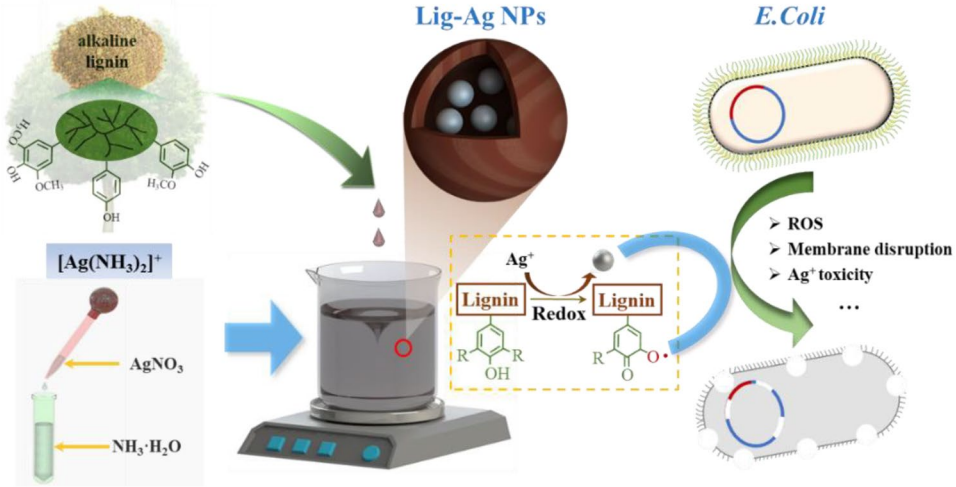

Fig. 1 The preparation and possible bactericidal process of Lig-Ag NPs

3 Result and discussion

3.1 Synthesis of Lig-Ag NPs

The environmentally friendly synthesis steps and theoretically bactericidal process of Lig-Ag NPs are shown in Fig. 1. Alkaline lignin was dissolved by NaOH and added into $[Ag(NH_3)_2]^+$ solution by dripping slowly. During mixture and blend, the methoxy (-OCH_3) and phenolic hydroxyl (-OH) were oxidized into quinone or semi-quinone free radicals. In the meantime, Ag^+ was reduced to form several Ag cores inside a lignin compact shell. The core–shell structure has some possible pathways to carry out bactericidal functions. Obviously, the Ag core could continually release silver ions and cross the lignin shell to influence the bacterial cells. On the other hand, the oxidized active groups (quinone and semi-quinone free radicals) dispersed on the surface of the shell might generate a mass of oxidative stress, which was an important approach to accelerate the death of bacterial. Hereinafter, a series of characterization, evaluation, and mechanism analysis experiments were accomplished to prove and discuss the above hypothesis.

3.2 Characterization of Lig-Ag NPs

The morphology characterization results of Lig-Ag NPs are demonstrated in Fig. 2. FE-SEM images (Fig. 2a, e) showed that Lig-Ag NPs possessed a regular spherical structure and uniform particle size. According to the result of DLS (Fig. 2f and Table S1), the effective diameter of Lig-Ag NPs was 53.2 nm, and the polydispersity was 0.216. Nanodimension gave the particles a small size effect, which might destroy the bacteria by perforation of the cell membrane in theory. The zeta potential of Lig-Ag NPs was − 62.7 mV due to the negatively charged functional groups (such as hydroxyl group) on the surface of Lig-Ag NPs, which might prevent them from touching bacterial cells on account of electrostatic repulsion. As shown in Fig. 2b, c, carbon and silver are densely distributed in the whole image. Although the colocalization

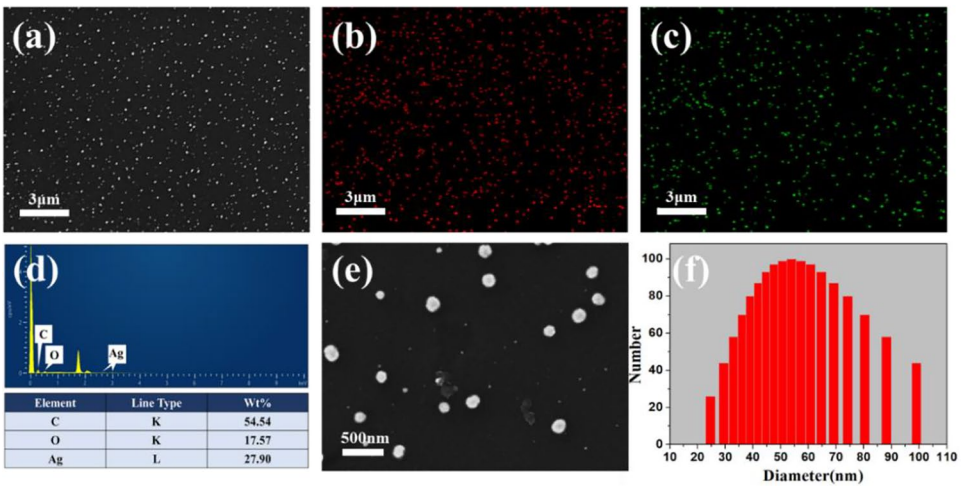

Element	Line Type	Wt%
C	K	54.54
O	K	17.57
Ag	L	27.90

Fig. 2 Morphology characterization of Lig-Ag NPs. (**a**, **e**) FE-SEM images of Lig-NPs, (**b**) element mapping of (**b**) carbon and (**c**) silver, (**d**) EDS spectra, and (**f**) DLS analysis of Lig-Ag NPs

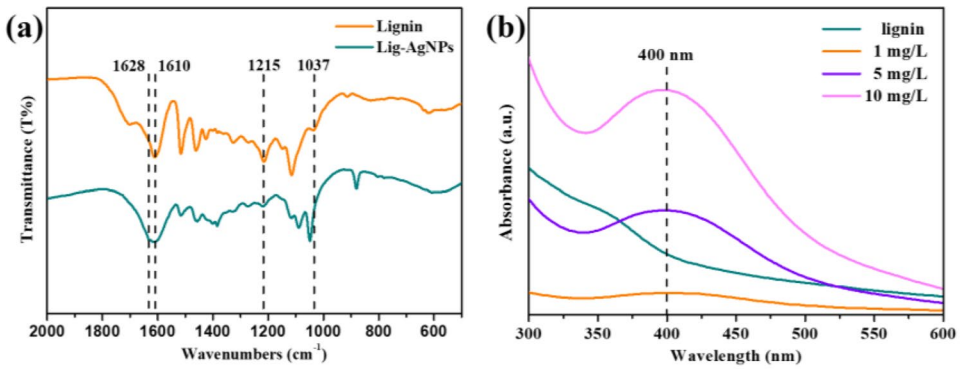

Fig. 3 (**a**) FT-IR and (**b**) UV–vis spectra of lignin and Lig-Ag NPs

phenomenon was hardly photographed due to the small size, the density of the elements presented an ideal encapsulation efficiency. For further quantitative analysis of element proportion, the total element content of distribution images is shown in Fig. 2d. The proportion of Ag, C, and O was 27.9%, 54.54%, and 17.57%, respectively, which indicated the volume ratio of lignin shell and Ag core. In addition, the wettability of Lig-Ag NPs was further investigated via WCA measurement. As shown in Fig. S1a, d, WCA are 48.4° and 55.8° when 1 mg/L Lig-Ag NPs and Ag NPs disperse over the surface of the polyamide membrane, respectively. These WCAs decreased to 36.7° (Fig. S1b) and 43.0° (Fig. S1e) when the concentrations of the materials were adjusted to 100 mg/L. WCA analysis results demonstrated that Lig-Ag NPs possessed well hydrophilicity, which endowed Lig-Ag NPs potential application in hydrophilic membrane and antibacterial wipes preparation.

FT-IR analysis was used to identify the oxidation of lignin functional groups. As depicted in Fig. 3a, the characteristic peaks at ~ 1610, ~ 1215, and ~ 1037 cm^{-1} correspond to the benzene ring bands, the phenolic hydroxyl (-OH) groups, and methoxy groups (-OCH_3) [41, 42]. The intensity of -OH and -OCH_3 peaks obviously decreased in the spectrum of Lig-Ag NPs compared with that of pure lignin. On the other hand, the characteristic peaks at ~ 1610 cm^{-1} were broadened due to the emergence of a new peak at ~ 1628 cm^{-1}, which corresponded to the carbanyl group (C = O) of quinone. FT-IR results indicated that the synthesis process of Lig-Ag NPs made the inherent groups (-OH and -OCH_3) of lignin oxidated to C = O along with the reduction of Ag^+ to Ag NPs. UV–vis analysis was used to characterize the surface plasmon resonance. In the UV–vis spectra (Fig. 3b), the enhancement of the quadrupole plasmon resonance was located in the region around 400 nm due to the presence of media interface between macromolecule (lignin) and metal (Ag NPs).

The information about the molecular structure of Lig-Ag NPs was further developed by XPS. As shown in Fig. 4, peak differentiation and fitting are operated in several narrowed ranges (C1s: 292–282 eV; Ag3d: 376–364 eV; O1s: 538–528 eV) of binding energy to study the valent state of carbon, silver, and oxygen [43–45]. The C1s spectra (Fig. 4b) showed an obvious decline in contents of C-O (286.1 eV) and a corresponding increase in the contents of C = O (288.1 eV). Similar variation trend of C-O (532.4 eV) and C = O (531.2 eV) contents was presented again in the spectra of O1s (Fig. 4d), which described the functional group change of lignin during the redox process particularly. On the other hand, Ag–O-Ag (530 eV) could ascribe to the hydrogen-bonding interaction between the Ag NPs and lignin. According to Fig. 4c, Ag 3d 3/2 and Ag 3d 5/2 peaks of Lig-Ag NPs arise at 373.2 eV and 367.2 eV, respectively. According to the XPS database (http://www.lasurface.com/), the above peaks were both ascribed to silver oxide (Ag_2O) which moved down compared with those of elemental Ag NPs (373.8 eV and 367.7 eV). These results of Ag3d described the changes of chemical environment around Ag atoms, which might be attributed to the capping lignin which electrostatically grafted to positively charge silver nanoclusters through ionogenic groups.

3.3 Effect of Lig-Ag NPs on bacterial culturability

Bacterial culturability experiments were carried out in PBS buffer, in which the bacteria cannot grow, but were viable. Firstly, *E. coli* were exposed to different concentrations of Lig-Ag NPs, and the bacterial survival graph was plotted. As depicted in Fig. 5a, a significant dosage effect of Lig-Ag NPs is observed. The percentage of bacteria survival was decreased as the concentration of Lig-Ag NPs and exposure time increased. Of particular note is the concentration of 5 mg/L and 10 mg/L of Lig-Ag NPs can kill more than 90% bacterial cells within 4 h (Fig. 5b) and completely killed 10^7 CFU/mL cells within 6 h. To display the bactericidal effect intuitively, the live bacteria colony on solid LB agar plates exposed to different Lig-Ag NPs concentrations within 4 h are photographed as shown in Fig. 5c.

Secondly, *E. coli* were exposed to comparable bactericidal materials with the same lignin or silver concentration, and the

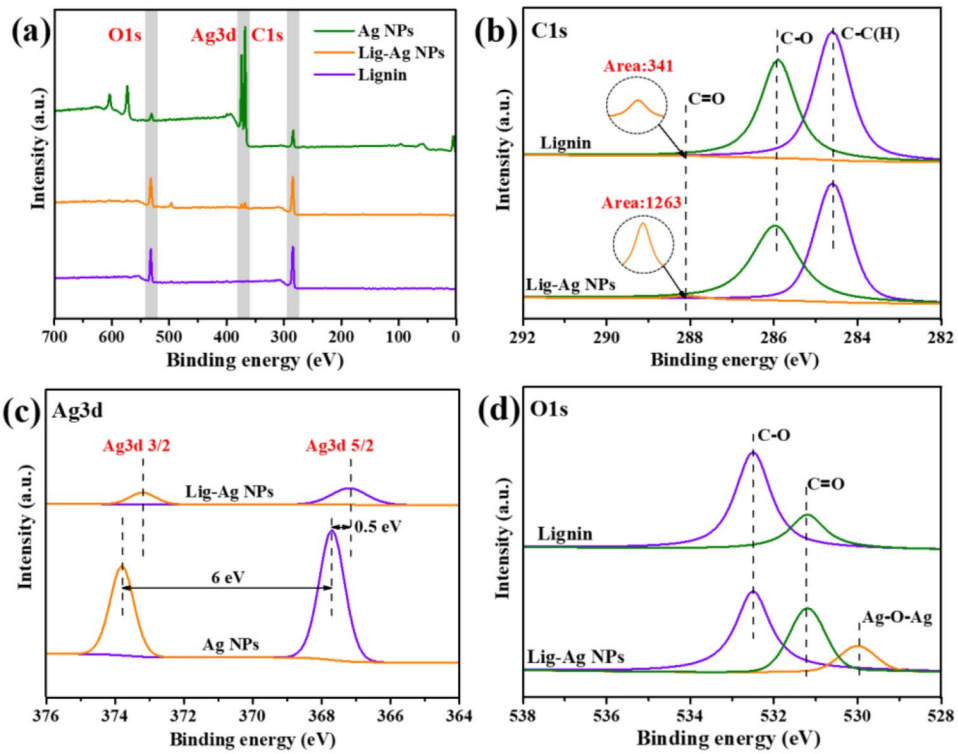

Fig. 4 XPS of Lig-Ag NPs, lignin, and Ag NPs. (**a**) Wide-scan XPS spectra. (**b**) high-resolution XPS of C1s for Lig-Ag NPs and lignin. (**c**) High-resolution XPS of Ag3d for Lig-Ag NPs and Ag NPs. (**d**) High-resolution XPS of O1s for Lig-Ag NPs and lignin

bacterial survival graph was plotted. As depicted in Fig. 5d, the bactericidal effect had a significant difference between Lig-Ag NPs and Ag NPs within the first 2 h. In this phase, 5 mg/L Lig-Ag NPs and Ag NPs can kill about 21% and 46% bacterial cells, respectively. However, these bactericidal effects were not invariable over time. In the performance attenuation experiments (Fig. 5e), after 3 months of storage, the bactericidal effect of Ag NPs suffered a significant decline due to the continuous consumption of silver ions. In contrast, that of Lig-Ag NPs had no significant change during storage.

The aforesaid sustaining bactericidal activity of Lig-Ag NPs might be derived from the core–shell structure. Outer lignin shell presented a barrier between inner silver core and bacteria, and mass transfer resistance of silver increased. Furthermore, a deeper question that needed to be discussed was the combined bactericidal mechanism. It was obvious that only the release process of silver ion cannot provide Lig-Ag NPs a comparable bactericidal effect compared with Ag NPs on account of lignin shell structure and electronegativity. Accordingly, cell membrane permeability, ROS scavenger experiments, and transcriptomic analysis were carried out to explore the combined bactericidal mechanism.

3.4 Effect of Lig-Ag NPs on membrane permeability of *E. coli*

Although the change of membrane permeability was unavoidable during cell death, the proportion of cells with a change in membrane permeability demonstrated the physical damage induced by Lig-Ag NPs. In these experiments, *E. coli* exposed to Ag NPs was set as a control group to analyze the degree of cell membrane damage. Syto9/PI dyes and flow cytometry were used to identify the membrane permeability at single-cell resolution. Briefly, the red fluorescent nucleic acid stain PI was used for identifying dead cells because it is supposed to penetrate only cells with disrupted membrane and is generally excluded from viable cells [40]. On the contrary, the green fluorescent Syto9 can enter both live and dead bacterial cells. Therefore, in the scatter diagram results (Fig. 6a–d), *X*-axis fluorescence intensity (Syto9) can be used to identify whether it is a bacterial cell or signal noise. On the other hand, *Y*-axis fluorescence intensity (PI) represented the permeability increase degree of the cell membrane. R1 and R2 oval regions were drawn artificially by graphical clustering analysis, in which the cells represented membrane damaged cells and membrane intact cells, respectively.

As shown in Fig. 6a, b, the membrane damaged cell proportions were 4.5% and 6% exposed to 1 mg/L Lig-Ag NPs and Ag NPs at 4 h, respectively. These proportions increased to 5.6% (Fig. 6c) and 21% (Fig. 6d) when the concentrations of the bactericidal materials were adjusted to 5 mg/L. Specifically, the ratios of R1/R2 were quantitatively analyzed. As shown in Fig. 6e, the membrane permeabilities are enhanced as the concentration of Lig-Ag NPs increased. However, compared with Ag NPs, the membrane permeability-increasing trend of Lig-Ag NPs was significantly slower. The possible

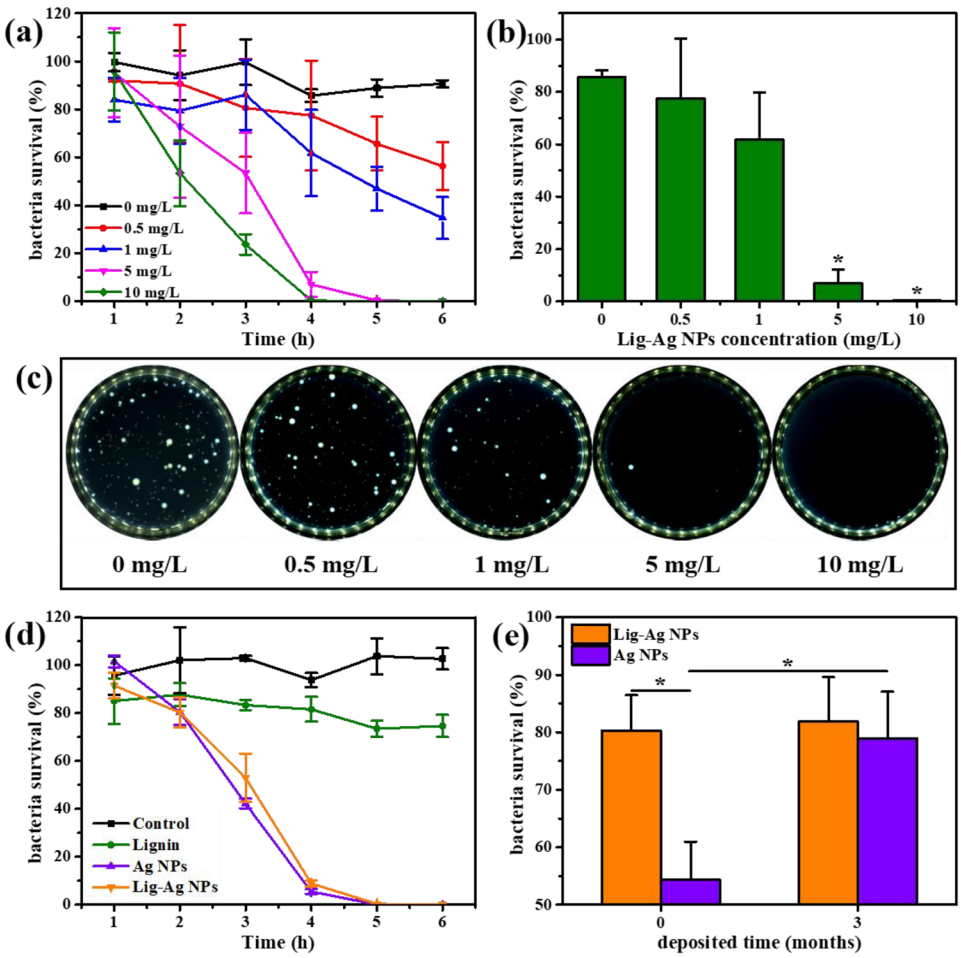

Fig. 5 Culturability loss of *Escherichia coli* induced by bactericidal materials exposure in PBS. (**a**) Variations in bacteria survival with different concentrations of Lig-Ag NPs within 6 h. (**b**) Variations in bacteria survival with different concentrations of Lig-Ag NPs for 4 h (*$p < 0.05$). (**c**) Photos of the live bacteria colony on solid LB agar plates exposure to different Lig-Ag NPs concentrations for 4 h. (**d**) Variations in bacteria survival with comparable concentration of Lig-Ag NPs (Ag-5 mg/L), Ag NPs (5 mg/L), and lignin (20 mg/L) within 6 h. (**e**) Variations in bacterial survival with Lig-Ag NPs and Ag NPs for 2 h before and after storage for 3 months (*$p < 0.05$)

cause for these results was the electronegativity of Lig-Ag NPs and bacterial cells which decreased the contact probability. To demonstrate the change of membrane permeability intuitively, the bacterial cell morphology was photographed exposed to

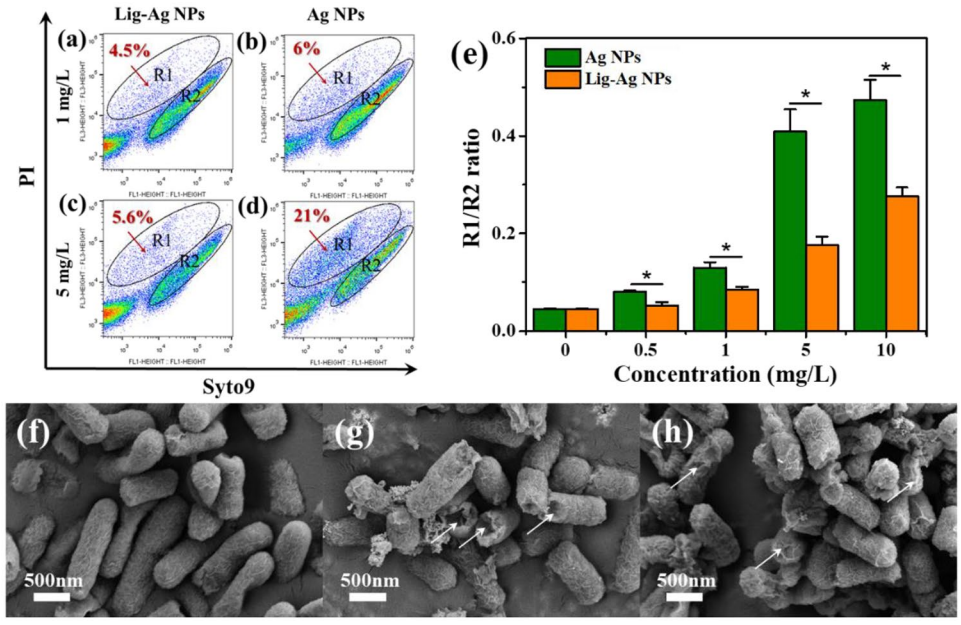

Fig. 6 Cell membrane permeability analysis of *E.coli* after 4 h exposure to specific concentration Lig-Ag NPs (**a** 1 mg/L, **c** 5 mg/L) and Ag NPs (**b** 1 mg/L, **d** 5 mg/L) by flow cytometry. (**e**) Variation in cell population ratio of R1/R2 with different concentration of bactericidal materials (*$p < 0.05$); FE-SEM images of *E. coli* after 4 h exposure to (**f**) PBS, (**g**) Ag NPs, and (**h**) Lig-Ag NPs

PBS (Fig. 6f), Ag NPs (Fig. 6g), and Lig-Ag NPs (Fig. 6h) at 4 h. PBS group presented *E. coli* cells with rhabditiform outline and unbroken membrane. The cells in the Ag NPs group had seriously damaged membrane, and bits of Ag NPs were attached to the membranes. The cell membrane morphology had also changed in Lig-Ag NPs groups. Different from the Ag NPs group, the membranes were atrophic and plicated instead of broken, which might be on account of the endogenous death process. As reported in our previous studies [16, 17, 46], it had been proved that nanomaterials could promote the transfer of antibiotic resistance genes by conjugation and transduction due to the increase of membrane permeability. Therefore, the decline in contact frequency and membrane broken degree was an ecological friendly characteristic of Lig-Ag NPs.

3.5 The combined bactericidal process of lignin and silver

It has been previously reported [18, 47, 48] that Ag NPs could induce oxidative stress, activate SOS response, and increase cell membrane permeability during the bactericidal process. In this work, we attempted to analyze the relevant bactericidal mechanism of Lig-Ag NPs at the gene expression level. As depicted in Fig. 7a and Table S2, Lig-Ag NPs and Ag NPs treatments result in a 1.3- and 1.8-fold increase in the expression of alkyl hydroperoxide reductase gene *ahpF*. The expression of *rutB* increased by 3.3- and 4.2-fold, and *soxS* exhibited a 4.7- and 5.3-fold increase in expression upon treatment with Lig-Ag NPs and Ag NPs, respectively. Of particular note was that the upregulation level of some genes (*hemH* [18], *rutD* [49], *sufA* [18], and *sufS* [18]) in Lig-Ag NPs group about ROS production was higher than that in the Ag NPs group. Moreover, Lig-Ag NPs and Ag NPs also increased the expression of SOS response related genes. These results indicated that Lig-Ag NPs-induced oxidative stress was a main mechanism in the bactericidal process. To further explore the bactericidal contribution of ROS production, ROS scavenger experiments were carried out. As shown in Fig. 7b, ROS scavenger blocks the process of oxidative stress and significantly weakens the bactericidal effect of Lig-Ag NPs and Ag NPs. The Lig-Ag NPs group with ROS scavengers no longer even had the bactericidal ability. These results demonstrated that oxidative stress was the leading bactericidal mechanism of Lig-Ag NPs.

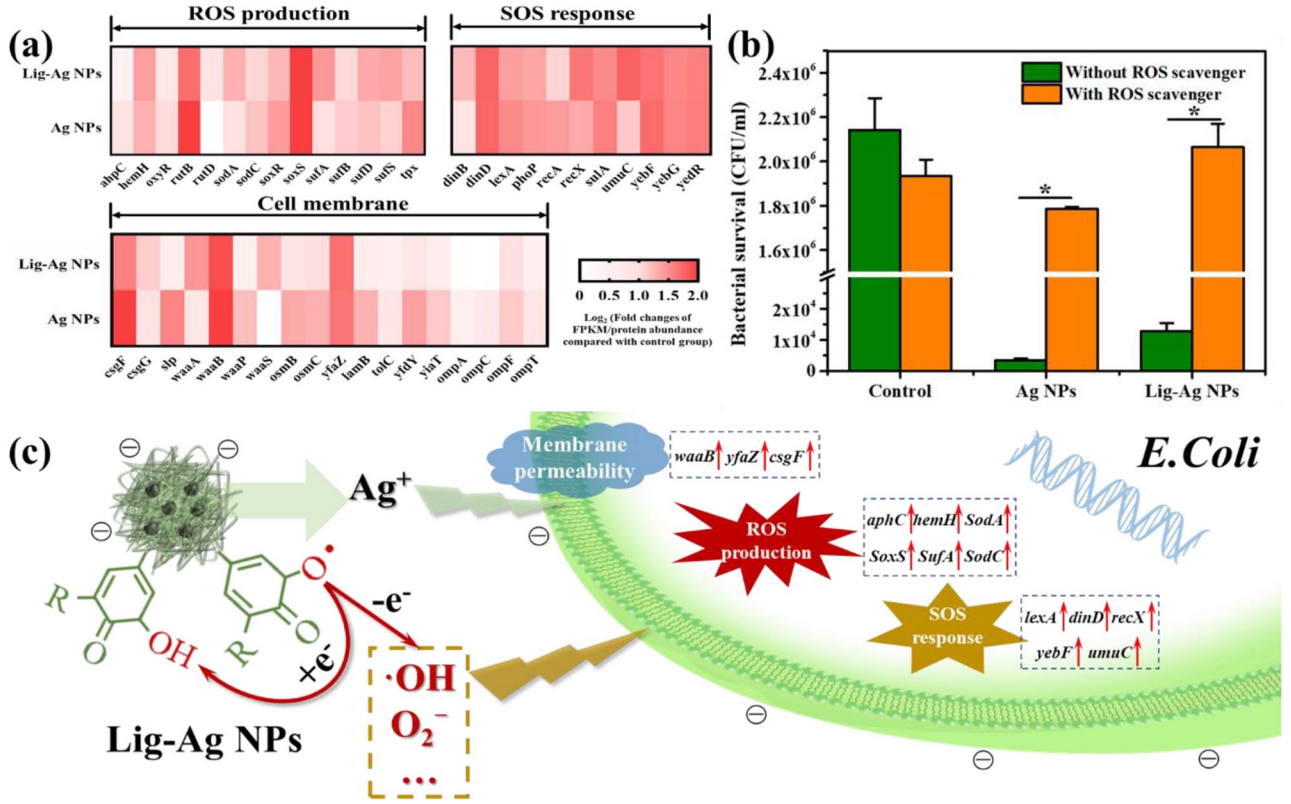

Fig. 7 (**a**) Fold changes in the expression of core genes related to ROS production, SOS response, and cell membrane permeability. (**b**) Variations in bacteria survival with the scavenger- and no scavenger-treated groups exposed to 5 mg/L Ag NPs and Lig-Ag NPs for 4 h (*$p < 0.05$). (**c**) Possible combined bactericidal mechanisms underlying *E. coli* exposed to Lig-Ag NPs

In addition, the expression of cell membrane permeability genes was investigated as well. The results showed that Lig-Ag NPs could also alter the transcription level of cell membrane related genes. For instance, the expression of *csgF* [49], *waaA* [18], *waaB* [18], and *yfaZ* [49] increased by ~ 3.0-fold when exposed to 5 mg/L Lig-Ag NPs. These genes are related to lipopolysaccharide synthesis (*waaA* and *waaB*) and putative outer membrane (*csgF* and *yfaZ*). Contrary to the ROS production results, the upregulation level of most genes about cell membrane in Lig-Ag NPs group was lower than that in Ag NPs group, which might be derived from the negative feedback of membrane damage being consistent with the results in Chapter 3.4.

Although oxidative stress was the possible leading bactericidal mechanism of Lig-Ag NPs, the formation approaches of ROS production are various on account of the combined effect of lignin and silver as depicted in Fig. 7c. Firstly, silver ion was slowly released and transferred across the lignin shell. This process might be accelerated on account of the negative charge surface, and the redox reaction between silver ion and a reducing group of lignin continuously proceed during the mass transfer process. In the meantime, quinone and semi-quinone radicals were consistently generated as intermediate products of the redox reaction. Secondly, these radicals could further generate reactive oxygen molecules such as hydroxyl radical (·OH), superoxide (O_2^-), and hole (h^+). Finally, whether these reactive oxygen molecules or silver ions were able to get inside the bacterial cells produce oxidative stress and inactivate them.

4 Conclusions

In this study, a simple and economic method was established to fabricate Lig-Ag NPs with bactericidal ability. Afterwards, materials characterization, bactericidal evaluation, and mechanism exploration were further implemented to explore the properties of Lig-Ag NPs. In summary, Lig-Ag NPs possessed a series of advantages. Firstly, the prepared Lig-Ag NPs demonstrated remarkable dispersity, uniformity, and encapsulation efficiency. Secondly, Lig-Ag NPs had approximated bactericidal ability compared with the same concentration of Ag NPs. Moreover, Lig-Ag NPs were endowed with better durability attributed to the core–shell structure and combined bactericidal mechanism. Last but not the least, Lig-Ag NPs were environmentally friendly which was not just from the green synthesis process, but also because theoretically lower ARGs transfer risk and environmental hypotoxicity due to lignin shell. In brief, this green hybrid nanoparticle would provide a new idea for the development of bactericidal materials.

Supplementary information The online version contains supplementary material available at https://doi.org/10.1007/s42114-022-00460-z.

Funding This study was funded by the Special Fund (grant numbers AWS18J004, 2019CXTD04, 20QNPY136, and 2019-JCJQ-JJ-163), the National Natural Science Foundation of China (grant numbers 51678565 and 42177414), and the Natural Science Foundation of Tianjin, China (grant number 19JCYBJC23800).

Declarations

Conflict of interest The authors declare no competing interests.

References

1. Kumar A, Goia DV (2020) Comparative analysis of commercial colloidal silver products. Int J Nanomedicine 15:10425–10434. https://doi.org/10.2147/IJN.S287730
2. Guner R, Hasanoglu I, Aktas F (2020) COVID-19: prevention and control measures in community. Turk J Med Sci 50 (SI-1):571–577. https://doi.org/10.3906/sag-2004-146
3. Azizi-Lalabadi M, Alizadeh-Sani M, Khezerlou A, Mirzanajafi-Zanjani M, Zolfaghari H, Bagheri V, Divband B, Ehsani A (2019) Nanoparticles and zeolites: antibacterial effects and their mechanism against pathogens. Curr Pharm Biotechnol 20(13):1074–1086. https://doi.org/10.2174/1573397115666190708120040
4. Fatima A, Yasir S, Ul-Islam M, Kamal T, Ahmad MW, Abbas Y, Manan S, Ullah MW, Yang G (2021) Ex situ development and characterization of green antibacterial bacterial cellulose-based composites for potential biomedical applications. Adv Compos Hybrid Mater. https://doi.org/10.1007/s42114-021-00369-z
5. Wu R, Wang W, Luo Q, Zeng X, Li J, Li Y, Li Y, Li J, Wang N (2021) Room temperature synthesis of defective cerium oxide for efficient marine anti-biofouling. Adv Compos Hybrid Mater. https://doi.org/10.1007/s42114-021-00256-7
6. He T, He J, Wang Z, Cui Z (2021) Modification strategies to improve the membrane hemocompatibility in extracorporeal membrane oxygenator (ECMO). Adv Compos Hybrid Mater 4(4):847–864. https://doi.org/10.1007/s42114-021-00244-x
7. Kaur A, Kumar R (2022) Untangling the effect of surfactants as an intermediate at gold nanoparticle-antibiotic interface for enhanced bactericidal effect. ES Food & Agroforestry. https://doi.org/10.30919/esfaf563
8. Guo J, Li X, Chen Z, Zhu J, Mai X, Wei R, Sun K, Liu H, Chen Y, Naik N, Guo Z (2022) Magnetic NiFe2O4/polypyrrole nanocomposites with enhanced electromagnetic wave absorption. J Mater Sci Technol 108:64–72. https://doi.org/10.1016/j.jmst.2021.08.049
9. Guo J, Chen Z, Xu X, Li X, Liu H, Xi S, Abdul W, Wu Q, Zhang P, Xu BB, Zhu J, Guo Z (2022) Enhanced electromagnetic wave absorption of engineered epoxy nanocomposites with the assistance of polyaniline fillers. Adv Compos Hybrid Mater. https://doi.org/10.1007/s42114-022-00417-2
10. Tang S, Zheng J (2018) Antibacterial activity of silver nanoparticles: structural effects. Adv Healthc Mater 7(13):e1701503. https://doi.org/10.1002/adhm.201701503
11. Richter AP, Brown JS, Bharti B, Wang A, Gangwal S, Houck K, Cohen Hubal EA, Paunov VN, Stoyanov SD, Velev OD (2015) An environmentally benign antimicrobial nanoparticle based on a silver-infused lignin core. Nat Nanotechnol 10(9):817–823. https://doi.org/10.1038/nnano.2015.141
12. Wang T, Wusigale KD, Amalaradjou MA, Luo Y, Luo Y (2021) Polydopamine-coated chitosan hydrogel beads for synthesis and immobilization of silver nanoparticles to simultaneously enhance antimicrobial activity and adsorption kinetics. Adv

Compos Hybrid Mater 4(3):696–706. https://doi.org/10.1007/s42114-021-00305-1
13. Kale SK, Parishwad GV, Patil ASNHAS (2021) Emerging agriculture applications of silver nanoparticles. ES Food & Agroforestry 3:17–22. https://doi.org/10.30919/esfaf438
14. Prasad SR, Teli SB, Ghosh J, Prasad NR, Shaikh VS, Nazeruddin GM, Al-Sehemi AGA, Patel I, Shaikh YI (2021) A review on bio-inspired synthesis of silver nanoparticles: their antimicrobial efficacy and toxicity. Eng Science 16:90–128. https://doi.org/10.30919/es8d479
15. Raghunath A, Perumal E (2017) Metal oxide nanoparticles as antimicrobial agents: a promise for the future. Int J Antimicrob Agents 49(2):137–152. https://doi.org/10.1016/j.ijantimicag.2016.11.011
16. Qiu Z, Yu Y, Chen Z, Jin M, Yang D, Zhao Z, Wang J, Shen Z, Wang X, Qian D, Huang A, Zhang B, Li JW (2012) Nanoalumina promotes the horizontal transfer of multiresistance genes mediated by plasmids across genera. Proc Natl Acad Sci U S A 109(13):4944–4949. https://doi.org/10.1073/pnas.1107254109
17. Ding C, Jin M, Ma J, Chen Z, Shen Z, Yang D, Shi D, Liu W, Kang M, Wang J, Li J, Qiu Z (2021) Nano-Al(2)O(3) can mediate transduction-like transformation of antibiotic resistance genes in water. J Hazard Mater 405:124224. https://doi.org/10.1016/j.jhazmat.2020.124224
18. Lu J, Wang Y, Jin M, Yuan Z, Bond P, Guo J (2020) Both silver ions and silver nanoparticles facilitate the horizontal transfer of plasmid-mediated antibiotic resistance genes. Water Res 169:115229. https://doi.org/10.1016/j.watres.2019.115229
19. Hu CC, Chang CH, Chang Y, Hsieh JH, Ueng SW (2020) Beneficial effect of TaON-Ag Nanocomposite titanium on antibacterial capacity in orthopedic application. Int J Nanomedicine 15:7889–7900. https://doi.org/10.2147/IJN.S264303
20. Ahmad MA, Aslam S, Mustafa F, Arshad U (2021) Synergistic antibacterial activity of surfactant free Ag-GO nanocomposites. Sci Rep 11(1):196. https://doi.org/10.1038/s41598-020-80013-w
21. Khan MI, Paul P, Behera SK, Jena B, Tripathy SK, Stålsby Lundborg C, Mishra A (2021) To decipher the antibacterial mechanism and promotion of wound healing activity by hydrogels embedded with biogenic Ag@ZnO core-shell nanocomposites. Chem Eng J 417:128025. https://doi.org/10.1016/j.cej.2020.128025
22. Guo Y-F, Fang W-J, Fu J-R, Wu Y, Zheng J, Gao G-Q, Chen C, Yan R-W, Huang S-G, Wang C-C (2018) Facile synthesis of Ag@ZIF-8 core-shell heterostructure nanowires for improved antibacterial activities. Appl Surf Sci 435:149–155. https://doi.org/10.1016/j.apsusc.2017.11.096
23. Guo J, Li X, Liu H, Young DP, Song G, Song K, Zhu J, Kong J, Guo Z (2021) Tunable magnetoresistance of core-shell structured polyaniline nanocomposites with 0-, 1-, and 2-dimensional nanocarbons. Adv Compos Hybrid Mater 4(1):51–64. https://doi.org/10.1007/s42114-021-00211-6
24. Hua J, Marcus B, Rol, Larsson L, Shi Y, (2022) Friction control of chitosan-Ag hydrogel by silver ion. ES Mater Manuf 16:30–36. https://doi.org/10.30919/esmm5f555
25. Sun Z, Fridrich B, de Santi A, Elangovan S, Barta K (2018) Bright side of lignin depolymerization: toward new platform chemicals. Chem Rev 118(2):614–678. https://doi.org/10.1021/acs.chemrev.7b00588
26. Zhang M, Du H, Liu K, Nie S, Xu T, Zhang X, Si C (2021) Fabrication and applications of cellulose-based nanogenerators. Adv Compos Hybrid Mater 4(4):865–884. https://doi.org/10.1007/s42114-021-00312-2
27. More AP (2021) Flax fiber–based polymer composites: a review. Adv Compos Hybrid Mater. https://doi.org/10.1007/s42114-021-00246-9
28. Zhang H, Zhong J, Liu Z, Mai J, Liu H, Mai X (2021) Dyed bamboo composite materials with excellent anti-microbial corrosion. Adv Compos Hybrid Mater 4(2):294–305. https://doi.org/10.1007/s42114-020-00196-8
29. Zhu E-Q, Xu G-F, Ye X-Y, Yang J, Yang H-Y, Wang D-W, Shi Z-J, Deng J (2021) Preparation and characterization of hydrothermally pretreated bamboo powder with improved thermoplasticity by propargyl bromide modification in a heterogeneous system. Adv Compos Hybrid Mater 4(4):1059–1069. https://doi.org/10.1007/s42114-021-00316-y
30. Culebras M, Collins GA, Beaucamp A, Geaney H, Collins MN (2022) Lignin/Si hybrid carbon nanofibers towards highly efficient sustainable Li-ion anode materials. Eng Science 17:195–203. https://doi.org/10.30919/es8d608
31. Xu T, Du H, Liu H, Liu W, Zhang X, Si C, Liu P, Zhang K (2021) Advanced nanocellulose-based composites for flexible functional energy storage devices. Adv Mater 33(48):2101368. https://doi.org/10.1002/adma.202101368
32. Liu R, Dai L, Zou Z, Si C (2018) Drug-loaded poly(L-lactide)/lignin stereocomplex film for enhancing stability and sustained release of trans-resveratrol. Int J Biol Macromol 119:1129–1136. https://doi.org/10.1016/j.ijbiomac.2018.08.040
33. Dai L, Lu J, Kong F, Liu K, Wei H, Si C (2019) Reversible photocontrolled release of bovine serum albumin by azobenzene-containing cellulose nanofibrils-based hydrogel. Adv Compos Hybrid Mater 2(3):462–470. https://doi.org/10.1007/s42114-019-00112-9
34. Atta OM, Manan S, Ul-Islam MU, Ahmed AAQ, Ullah MW, Yang G (2021) Silver decorated bacterial cellulose nanocomposites as antimicrobial food packaging materials. ES Food & Agroforestry 6:12–26. https://doi.org/10.30919/esfaf590
35. Liu W, Du H, Zhang M, Liu K, Liu H, Xie H, Zhang X, Si C (2020) Bacterial cellulose-based composite scaffolds for biomedical applications: a review. ACS Sustain Chem Eng 8(20):7536–7562. https://doi.org/10.1021/acssuschemeng.0c00125
36. Chen J, An L, Bae JH, Heo JW, Han SY, Kim YS (2021) Green and facile synthesis of aminated lignin-silver complex and its antibacterial activity. Ind Crops Prod 173:114102. https://doi.org/10.1016/j.indcrop.2021.114102
37. Li M, Jiang X, Wang D, Xu Z, Yang M (2019) In situ reduction of silver nanoparticles in the lignin based hydrogel for enhanced antibacterial application. Colloids Surf, B 177:370–376. https://doi.org/10.1016/j.colsurfb.2019.02.029
38. Liu S, Du H, Liu K, Ma M-G, Kwon Y-E, Si C, Ji X-X, Choi S-E, Zhang X (2021) Flexible and porous Co3O4-carbon nanofibers as binder-free electrodes for supercapacitors. Adv Compos Hybrid Mater 4(4):1367–1383. https://doi.org/10.1007/s42114-021-00344-8
39. Farooq M, Zou T, Valle-Delgado JJ, Sipponen MH, Morits M, Österberg M (2020) Well-defined lignin model films from colloidal lignin particles. Langmuir 36(51):15592–15602. https://doi.org/10.1021/acs.langmuir.0c02970
40. Stiefel P, Schmidt-Emrich S, Maniura-Weber K, Ren Q (2015) Critical aspects of using bacterial cell viability assays with the fluorophores SYTO9 and propidium iodide. BMC Microbiol 15:36. https://doi.org/10.1186/s12866-015-0376-x
41. Dai L, Zhu W, Lu J, Kong F, Si C, Ni Y (2019) A lignin-containing cellulose hydrogel for lignin fractionation. Green Chem 21(19):5222–5230. https://doi.org/10.1039/c9gc01975h
42. Dai L, Liu R, Si C (2018) A novel functional lignin-based filler for pyrolysis and feedstock recycling of poly(l-lactide). Green Chem 20(8):1777–1783. https://doi.org/10.1039/c7gc03863a
43. Sanad MMS, Farahat MM, El-Hout SI, El-Sheikh SM (2021) Preparation and characterization of magnetic photocatalyst from the banded iron formation for effective photodegradation of methylene blue under UV and visible illumination. J Environ Chem Eng 9(2):105127. https://doi.org/10.1016/j.jece.2021.105127
44. Kumar AS, Sornambikai S, Gayathri P, Zen J-M (2010) Selective covalent immobilization of catechol on activated carbon electrodes. J

Electroanal Chem 641(1):131–135. https://doi.org/10.1016/j.jelechem.2009.12.016
45. Boronin AI, Koscheev SV, Zhidomirov GM (1998) XPS and UPS study of oxygen states on silver. J Electron Spectrosc Relat Phenom 96(1):43–51. https://doi.org/10.1016/S0368-2048(98)00221-7
46. Qiu Z, Shen Z, Qian D, Jin M, Yang D, Wang J, Zhang B, Yang Z, Chen Z, Wang X, Ding C, Wang D, Li JW (2015) Effects of nano-TiO2 on antibiotic resistance transfer mediated by RP4 plasmid. Nanotoxicology 9(7):895–904. https://doi.org/10.3109/17435390.2014.991429
47. Almatroudi A (2020) Silver nanoparticles: synthesis, characterisation and biomedical applications. Open Life Sci 15(1):819–839. https://doi.org/10.1515/biol-2020-0094
48. Park HJ, Kim JY, Kim J, Lee JH, Hahn JS, Gu MB, Yoon J (2009) Silver-ion-mediated reactive oxygen species generation affecting bactericidal activity. Water Res 43(4):1027–1032. https://doi.org/10.1016/j.watres.2008.12.002
49. Wang Y, Lu J, Mao L, Li J, Yuan Z, Bond PL, Guo J (2019) Antiepileptic drug carbamazepine promotes horizontal transfer of plasmid-borne multi-antibiotic resistance genes within and across bacterial genera. ISME J 13(2):509–522. https://doi.org/10.1038/s41396-018-0275-x